Journal of Hazardous Materials 302 (2016) 1–9

Contents lists available at ScienceDirect

Journal of Hazardous Materials

journal homepage: www.elsevier.com/locate/jhazmat

Immobilization of uranium by biomaterial stabilized FeS nanoparticles: Effects of stabilizer and enrichment mechanism

Dadong Shao[a,b], Xuemei Ren[b,*], Jun Wen[a], Sheng Hu[a], Jie Xiong[a], Tao Jiang[a], Xiaolin Wang[c,*], Xiangke Wang[d,*]

[a] Institute of Nuclear Physics and Chemistry, China Academy of Engineering Physics, Mianyang 621900, PR China
[b] Institute of Plasma Physics, Chinese Academy of Sciences, P.O. Box 1126, Hefei 230031, PR China
[c] China Academy of Engineering Physics, Mianyang 621900, PR China
[d] School of Environment and Chemical Engineering, North China Electric Power University, Beijing 102206, PR China

HIGHLIGHTS

- FeS can be stabilized by sodium carboxymethyl cellulose and gelatin.
- Gelatin–FeS show best performance in U(VI) removal.
- Adsorption–reduction immobilization of U(VI) is the major mechanism.

GRAPHICAL ABSTRACT

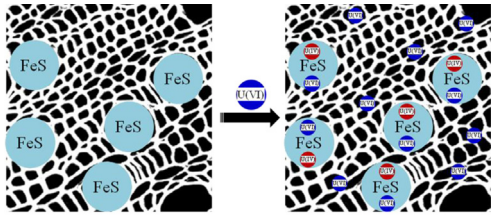

ARTICLE INFO

Article history:
Received 16 June 2015
Received in revised form 4 September 2015
Accepted 21 September 2015
Available online 25 September 2015

Keywords:
Stabilized FeS
Immobilization mechanisms
Uranium
Biomaterial
Radioactive wastewater

ABSTRACT

Iron sulfide (FeS) nanoparticles have been recognized as effective scavengers for multi-valent metal ions. However, the aggregation of FeS nanoparticles in aqueous solution greatly restricts their application in real work. Herein, different biomaterial-FeS nanoparticles were developed for the in-situ immobilization of uranium(VI) in radioactive waste management. TEM images suggested that sodium carboxymethyl cellulose (CMC) and gelatin can effectively suppress the aggregation of FeS nanoparticles in aqueous solutions. The resulting CMC–FeS and gelatin–FeS were stable in aqueous solutions and showed high adsorption capacity for U(VI). Specially, gelatin–FeS showed the best performance in U(VI) adsorption–reduction immobilization under experimental conditions. The maximum enrichment capacity of U(VI) on CMC–FeS and gelatin–FeS at pH 5.0 and 20 °C achieved to ~430 and ~556 mg/g, respectively. Additionally, gelatin–FeS and CMC–FeS nanoparticles presented excellent tolerance to environmental salinity. The immobilized U(VI) on the surfaces of CMC–FeS and gelatin–FeS remained stable more than one year. These findings highlight the possibility of using ggelatin–FeS for efficient immobilization of U(VI) from radioactive wastewater.

© 2015 Elsevier B.V. All rights reserved.

1. Introduction

With the fast development of nuclear technique during the past decades, large quantities of radioactive wastewater were produced [1–3]. Uranium, a fundamental and essential material of nuclear technique, is widely considered as one of the most important contaminates in radioactive wastewater [4]. Its release into

* Corresponding authors. Fax: +86 551 65591310.
E-mail addresses: renxm_nana@163.com (X. Ren), xlwang@caep.ac.cn (X. Wang), xkwang@ncepu.edu.cn (X. Wang).

http://dx.doi.org/10.1016/j.jhazmat.2015.09.043
0304-3894/© 2015 Elsevier B.V. All rights reserved.

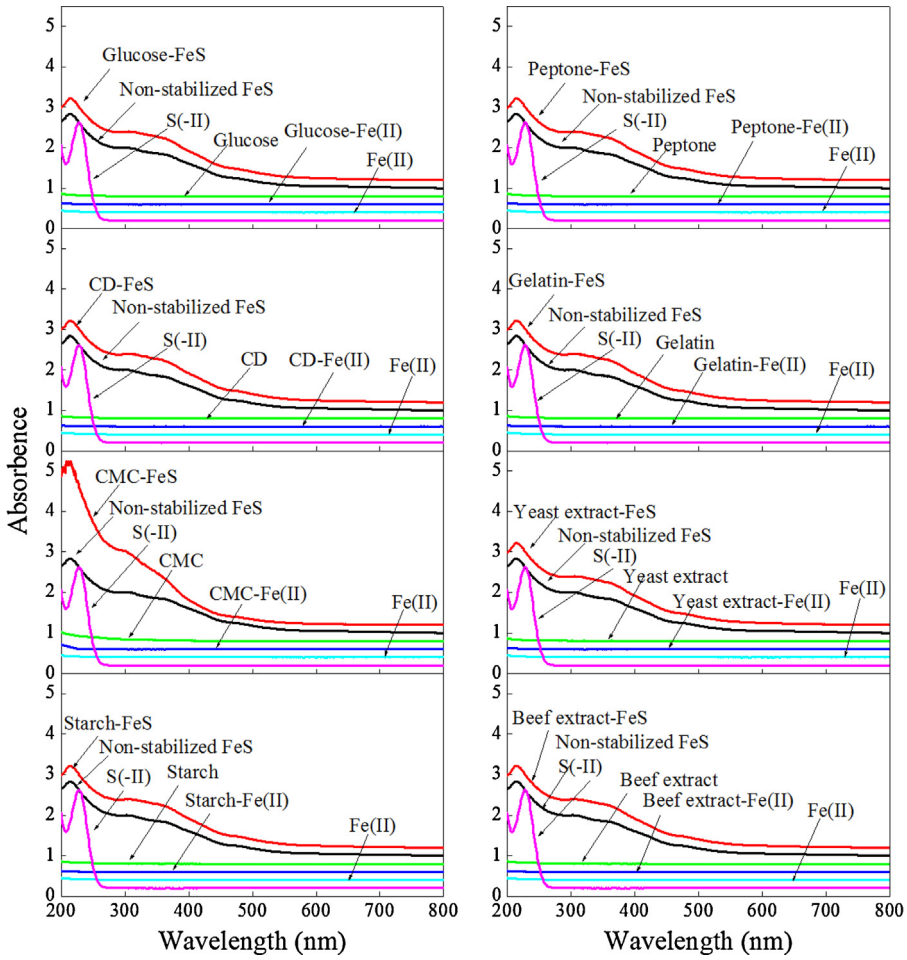

Fig. 1. UV–vis spectra of 50 mg/L biomaterials, 5.7 mmol/L Fe(II), 5.7 mmol/L Na_2S, biomaterial-Fe(II) complexes (50 mg/L biomaterials and 5.7 mmol/L Fe(II)), 50 mg/L bare FeS, and 50 mg/L biomaterial-FeS nanoparticles (50 mg/L biomaterials and 50 mg/L FeS).

environment can cause serious pollution. The effective enrichment and separation of uranium from radioactive wastewater is an important science issue for the sustainable development of nuclear energy. The environmental risk of uranium is dependent on its redox state: soluble U(VI) species dominate under oxidizing conditions and sparingly soluble U(IV) species dominate under reducing conditions [1,5–7]. Researchers widely believe that the reductive immbolization of U(VI) is as an effective method for comprehensive management of U(VI) contaminants [7,8]. Naturally occurring FeS minerals and synthetic bulk FeS materials have been widely used as an effective abiotic reducing agent for uranium management [6,7,9–11].

Because of their larger specific surface area and potentially more active reaction sites, nanoscale FeS materials are expected to present much higher immbolization capacity as compared to FeS minerals or bulk FeS materials. However, due to van der Waals interaction [12–14], bare FeS nanoparticles have a strong tendency to form large aggregates [15]. In order to reduce the aggregation of FeS nanoparticles, significant advances have focused on the exploration of stabilizer with effective stabilization capacity for FeS nanoparticles. Using biomaterials as stabilizer have attracted considerable attention because of their specific properties, such as biodegradability, abundant functional groups and low production cost. The application of CMC as pre-agglomeration stabilizer was proved to be a feasible approach to synthesize FeS nanoparticles with highly stable and soildeliverable [12,15]. The present CMC molecules are believed to complex Fe(II) and thereby disperse Fe(II) throughout CMC network before the formation of FeS nanoparticles [16–18]. Moreover, CMC molecules form a bulky and negatively charged layer on nanoparticle surfaces [17], which provide strong steric repulsions and/or interparticle electrostatic repulsions to limit the growth of FeS nanoparticles. Meanwhile, starch [19,20] and cyclodextrin (CD) [21] can also effectively stabilize nanoparticles, such as FeS, zero valent iron, Fe_3O_4, etc. The stabilized particles displayed excellent stability and reactivity as compared with bare FeS nanoparticles. However, to our best knowledge, the comprehensive investigation of the common biomaterials as stabilizer of FeS are still fragmented and limited. Herein, CMC, CD, starch, glucose, beef extract, gelatin, peptone, and yeast extract were selected as the representative of plant and animal derived biomaterials and used as the stabilizer of FeS nanoparticles. Stabilized FeS nanoparticles were synthesized by chemical coprecipitation technique in the presence of biomaterials and applied as adsorbent to effectively immbolize U(VI) from aqueous solutions under a variety of solution conditions.

The overall goal of this paper was to explore new biomaterial with excellent stabilization capacity for FeS nanoparticles, and to investigate the performance of stabilized and modified FeS in U(VI) immobilization. The specific objectives are to: (1) prepare various biomaterial-FeS nanoparticles and compare the effectiveness of stabilization capacity of different biomaterials; (2) examine the effect of operation conditions on the enrichment of U(VI) by stabilized biomaterial-FeS nanoparticles in detail; (3) elucidate the immbolization mechanism of U(VI) on stabilized biomaterial-FeS nanoparticles; and (4) examine long-term stability of U(VI) immobilized by stabilized biomaterial-FeS nanoparticles.

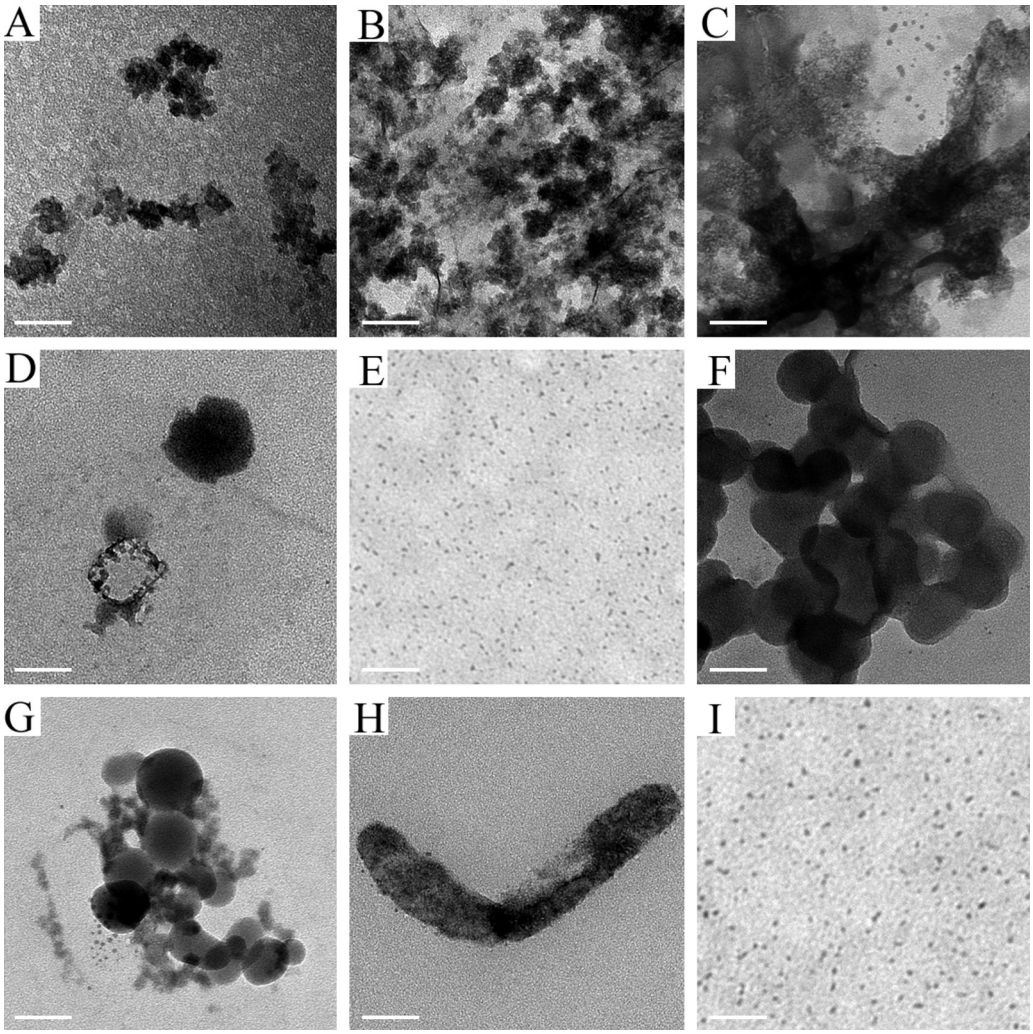

Fig. 2. TEM images of FeS without stabilizer (A) and with different biomaterials as stabilizer (500 mg/L), including glucose (B), CD (C), starch (D), CMC (E), yeast extract (F), beef extract (G), peptone (H) and gelatin (I). The scale bars represent 100 nm.

2. Experimental

2.1. Materials

Biomaterial-FeS nanoparticles (70 mL) were synthesized based on the reaction of Na_2S with $FeCl_2$ in the presence of biomaterials [15]. Briefly, under continuous magnetic stirring condition, the certain amounts of biomaterial solution (1.0 g/L), Milli-Q water, and 10.0 mL $FeCl_2$ (0.040 mol/L) solution were added into three-necked flasks to yield the desired concentrations of Fe(II) and stabilizers. After purged with high purity argon for 1 h, stoichiometric amounts of Na_2S solution (0.040 mol/L) were added dropwise to produce FeS nanoparticles. The resulted suspensions containing 0.50 g/L FeS and desired amount of stabilizers were sealed and aged for 24 h to ensure the full growth of biomaterial-FeS nanoparticles. For comparison, bare FeS nanoparticles were also prepared following the same procedure except no stabilizer was used.

2.2. Characterization

The physiochemical properties of biomaterial-FeS nanoparticles were measured and evaluated by a high-resolution transmission electron microscope (HR-TEM), viscosity measurements, UV–vis spectroscopy, and X-ray photoelectron spectroscopy (XPS) in detail. The TEM images were performed on a Hitachi HT-7700 TEM microscope. The viscosity of biomaterial-FeS solution was measured with a Brookfield viscometer model DV-III. UV–vis spectrophotometer analysis was mounted on a Shimadzu 2550 UV–vis spectrophotometer. XPS measurements were performed with an ESCALab220i-XL surface microanalysis system (VG Scientific) equipped with an Al Ka ($h\nu$ = 1486.6 eV) source at a chamber pressure of 3×10^{-9} mbar. The surface charging effects were corrected with C 1s peak at 284.4 eV as a reference. For XPS analysis, FeS nanoparticles were collected by centrifugation the suspensions at 18,000 rpm for 30 min (BECKMAN COULTER 64R) at 20 °C, and subsequently freeze dried under vacuum.

2.3. Batch experiment

In order to evaluate the effect of different biomaterials on FeS adsorption capacity, the enrichment of U(VI) from aqueous solution on biomaterial-FeS were studied at 20 ± 1 °C by using batch technique under nitrogen conditions. The bulk suspensions of adsorbent and NaCl solution were added into polyethylene test tubes and pre-equilibrated for 24 h, then U(VI) solution and Milli-Q water was added to achieve the desired concentrations of different components, and the pH of suspensions were adjusted to the desired values by adding negligible volumes of 0.1 or 0.01 mol/L HCl or NaOH. It is noteworthy that several hours were enough to achieve the adsorption equilibration in kinetic experiments. In order to

achieve the adsorption equilibrium, the suspensions were shaken for 48 h to achieve the adsorption equilibration. The solid and liquid phases were separated by centrifugation at 18,000 rpm for 30 min (BECKMAN COULTER 64R) at 20 °C. The final concentration (C_e, mg/L) of U(VI) in supernatant was analyzed by arsenazo III spectrophotometric method at 650 nm. The adsorption percents of U(VI) were calculated from the difference between the initial concentration (C_0, mg/L) and C_e (mg/L). All of the experimental data were the averages of triplicate determinations. The relative errors of data were <5%.

3. Results and discussions

3.1. Effects of biomaterial type and concentration on FeS stability

UV–vis spectra in Fig. 1 provide a convenient evidence of the formation of biomaterial-FeS nanoparticles. The individual solutions of Fe(II), Na_2S, biomaterials, and biomaterial-Fe(II) complexes appeared clear and colorless, and no absorbance peak was observed at wavelength >250 nm. After the additional of Na_2S, the solutions of Fe(II) and biomaterial-Fe(II) complexes turned black and turbid, resulting in strong absorbance profile in the broad wavelength range of 200–800 nm. Due to a change in the local refractive index around the particles caused by the bound biomaterials surrounding the nanoparticles, the shifts in absorbance peaks of biomaterial-FeS suspensions were observed as compared to naked FeS suspensions [22]. The UV–vis spectra of biomaterial-FeS suspensions in sealed quartz micro-plates were monitored for 24 h. No notable change in the UV–vis spectra of CMC–FeS and gelatin–FeS was detected, indicating the excellent physically and chemically stabilization of CMC–FeS and gelatin–FeS nanoparticles in aqueous solutions [23].

Fig. 2 shows the TEM images of FeS nanoparticles (0.5 g/L) without stabilizer (A) and with different biomaterials as stabilizer (0.5 g/L), including glucose (B), CD (C), starch (D), CMC (E), yeast extract (F), beef extract (G), peptone (H) and gelatin (I). All FeS nanoparticles were sonicated for 10 min before TEM imaging. Due to van der Waals interactions [12], bare FeS nanoparticles aggregated into large agglomerates and appeared like a large flocs. Evidently, the present of CMC and gelatin in aqueous solution can effectively suppress the growth and aggregation of FeS nanoparticles in aqueous solutions under experimental conditions. And the CMC–FeS and gelatin–FeS nanoparticles appeared clearly discrete. A lot of researchers [12,15,23] reported similar results, which showed that the co-existing CMC can prevent the agglomeration of FeS nanoparticles. The previous Fourier transform infrared spectroscopy study of CMC-stabilized FeS nanoparticles [15] suggested that negatively charged CMC stabilized the FeS nanoparticles by the concurrence of electrostatic repulsion and steric hindrance, and the attachment of CMC molecules to the FeS nanoparticles through carboxylate and hydroxyl groups in forms of bidentate bridging facilitated the stabilization of the FeS nanoparticles. Similarly, the FeS nanoparticles attached to the gelatin chain via electrostatic interaction and the special interaction between hydroxyl (—OH) groups of FeS and amino (—NH_2) and carboxyl (—COOH) groups of gelatin, and electrostatic repulsion and polymeric chain of gelatin protected the FeS nanoparticles from aggregation [24]. In our case, other studied biomaterials as stabilizer did not present superior stabilization capacity. Additionally, the viscosities were measured to be 1.04, 1.07, 1.07, 1.13, 1.42, 1.15, 1.13, 1.11, and 1.45 mPa s for bare FeS, glucose–FeS, CD–FeS, starch–FeS, CMC–FeS, yeast extract–FeS, beef extract–FeS, peptone–FeS, and gelatin–FeS, respectively. Based on the report of Sakulchaicharoen et al. [16], the increased suspension viscosity also contributed to the enhanced nanoparticle stability by slowing down the Brownian motion that leads to the agglomeration.

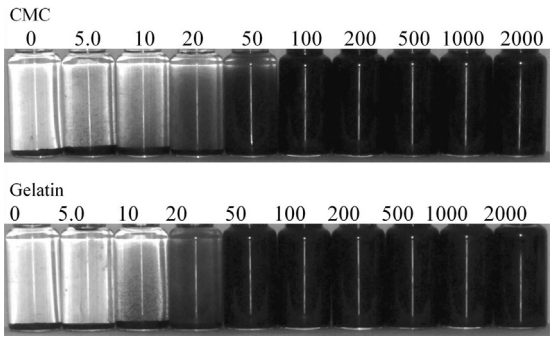

Fig. 3. Photographs of CMC and gelatin concentrations (0–2000 mg/L) effects on the dispersion and stabilization of FeS particles. FeS particles were prepared in aqueous solutions at FeS = 500 mg/L in both cases, and were stood for 24 h.

Fig. 3 straightly demonstrates the effects of CMC and gelatin concentrations on the dispersion of FeS nanoparticles in aqueous solutions. After standing for 24 h, bare FeS nanoparticles precipitated at the bottom of bottle by gravity, while the precipitation of FeS nanoparticles decreased with increasing CMC and gelatin concentrations. The fully stabilized FeS nanoparticles can be achieved when CMC and gelatin concentrations attained to 0.1 and 0.05 g/L (i.e. the weight ratios were 0.2 for CMC-to-FeS and 0.01 for gelatin-to-FeS), respectively. Thus, 0.1 and 0.05 g/L were regarded as the

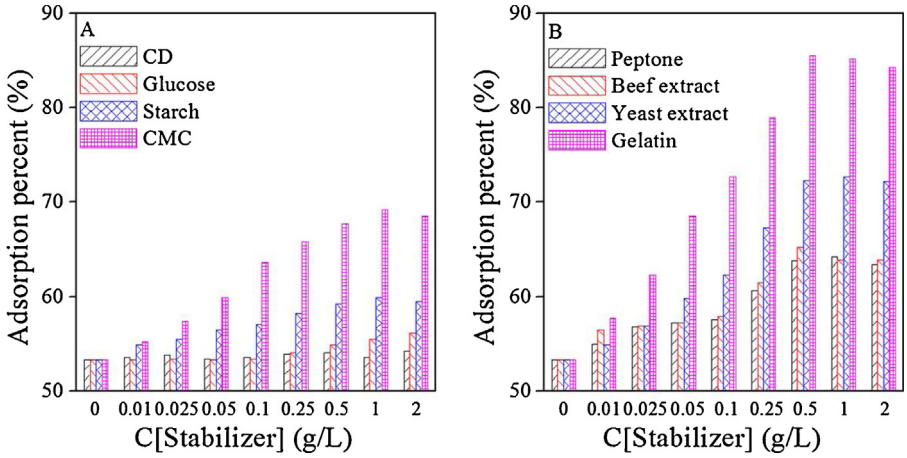

Fig. 4. U(VI) uptake by biomaterial-FeS nanoparticles prepared at various biomaterial concentrations derived from plants (A) and animals (B). $T = 20 \pm 1$ °C, contact time: 48 h, $C[U(VI)]_{(initial)} = 50.0$ mg/L, $C[FeS] = 100.0$ mg/L, pH 5.0 ± 0.1, $C[NaCl] = 0.10$ mol/L.

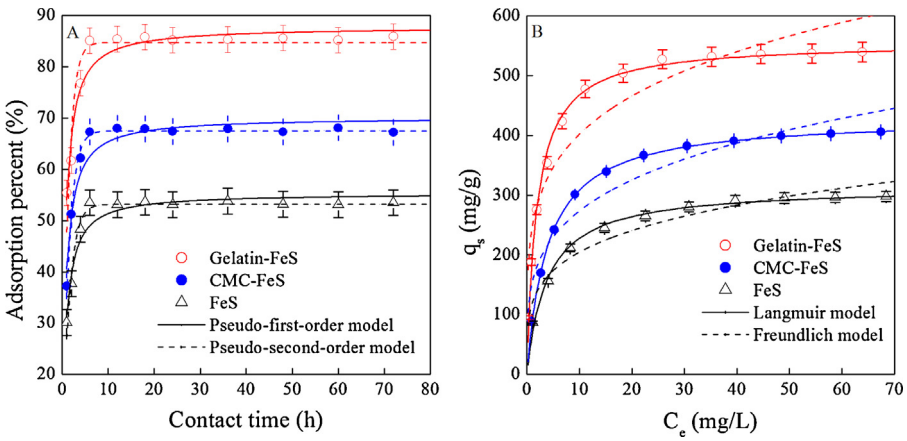

Fig. 5. (A) Effect of contact time on U(VI) uptake by naked FeS, CMC–FeS, and gelatin–FeS nanoparticles. (B) The enrichment performance of naked FeS, CMC–FeS, and gelatin–FeS nanoparticles in U(VI) uptake. $T = 20 \pm 1$ °C, C[FeS] = 100.0 mg/L, pH 5.0 ± 0.1, C[NaCl] = 0.10 mol/L. (A) $C[U(VI)]_{(initial)}$ = 50.0 mg/L. (B) Contact time: 48 h.

minimum concentrations of CMC and gelatin that needed to fully stabilize FeS nanoparticles, respectively. In our case, the stabilizing ability of gelatin was higher than that of CMC, which indicated that the amino (—NH_2) groups in gelatin may play an important role in stabilizing FeS nanoparticles. This needed to be further elucidated in future. Almeida et al. [25] and Gaihre et al. [26] also found that the chemisorbed polymeric chain of gelatin on $NiMn_2O_4$ and Fe_3O_4 nanoparticles can protect the nanoparticles from aggregation. It is worth noting that Gong et al. [15] reported that after standing for 24 h, ~97% bare FeS nanoparticles were precipitated by gravity, while all CMC–FeS nanoparticles were remained in supernatant when CMC concentration is 0.3 g/L or higher. The potential reasons for different results between Gong et al. [15] and our work are the preparation method and the properties of used CMC and FeS.

3.2. Effect of biomaterial type and concentration on U(VI) immobilization capability

Fig. 4 shows effect of biomaterial type and concentration on the enrichment capability of biomaterial-FeS nanoparticles for U(VI). Evidently, U(VI) adsorption on biomaterial-FeS nanoparticles increased with increasing biomaterial concentrations to ~0.5 g/L, and then slightly decreased with further increasing biomaterial concentrations. The related biomaterial-to-FeS weight ratios were determined to be ~1.0:1, which was used in the subsequent tests. Gong et al. [15] also reported similar changing trends, and the optimum adsorption capacity of CMC–FeS for Hg(II) was achieved at CMC-to-FeS weight ratio of ~1.0:1. Increasing biomaterial concentration not only can reduce the average size of FeS aggregation, which would improve the specific surface area and sorption sites of FeS, but also can provide more functional groups from biomaterial for binding contaminants, and consequently facilitate contaminant removal. However, with further increasing biomaterial concentration, the excessive amount of biomaterials surrounding FeS surface can inhibit the accessing of contaminants to the surface of FeS nanoparticles. In our case, gelatin–FeS nanoparticles present highest enrichment capability for U(VI) under same experimental conditions, followed by CMC–FeS nanoparticles. It indicated that besides CMC, gelatin can also be used as an effective stabilizer for FeS nanoparticles. Furthermore, gelatin–FeS nanoparticles showed better performance in enrichment capability for U(VI). Since the abundant —NH_2 and —COOH groups in gelatin, an important natural macromolecule derived from animal proteins, [27] can effectively improve the adsorption capacity of nano-materials for metal ions, [28] drags, [29] and organic contaminants [30]. It is clear that FeS nanoparticle stabilization technique not only reduces its aggregation in aqueous solutions, but also increases its enrichment capacity. In the following part, we chose CMC–FeS and gelatin–FeS nanoparticles as examples for studying the immobilization of U(VI) on biomaterial-FeS nanoparticles in detail.

Table 1
Kinetic parameters of pseudo-first-order and pseudo-second-order kinetic models.

	Pseudo–first–order model			Pseudo–second–order model		
	q_e (mg/g)	k_1 (1/h)	R^2	q_e (mg/g)	k_2 (mg/g h)	R^2
FeS	266	0.706	0.967	269	4860	0.999
CMC–FeS	338	0.744	0.991	340	4800	0.999
Gelatin–FeS	428	0.831	0.886	431	3130	0.999

3.3. Adsorption kinetics, isotherms, and mechanisms of U(VI) on CMC–FeS and gelatin–FeS

3.3.1. Adsorption kinetics

Equilibrium time is one of the important operational parameters for an economical wastewater treatment plant. The effects of contact time on U(VI) adsorption onto FeS, CMC–FeS, and gelatin–FeS nanoparticles are shown in Fig. 5A. The adsorption of U(VI) on FeS, CMC–FeS and gelatin–FeS were rapid in the initial 1 h of contact time, and then maintained level with further increasing contact time. And ~6 h were enough to achieve the adsorption equilibrium. Gong et al. [15] also reported that the immobilization of Hg(II) by CMC–FeS achieved the equilibrium at ~6.7 h. The initial fast adsorption of U(VI) on FeS might be due to its nanoscale particle size, since fine particles are favorable for the diffusion of U(VI) from bulk solution onto the active sites of the adsorbents [31]. Additionally, the abundant functional groups like —COOH groups from CMC and —NH_2 and —COOH groups from gelatin attributed to the quick adsorption of U(VI) on CMC–FeS and gelatin–FeS.

To investigate the mechanism of adsorption kinetics, the pseudo-first-order kinetic model ($\ln(q_e - q_t) = \ln q_e - k_1 t$, where k_1 is the rate constant of pseudo-first-order model, q_e and q_t are the amount of U(VI) adsorbed onto adsorbents at equilibrium and at any time t (h), respectively) and pseudo-second-order kinetic model ($t/q_t = 1/(2k_2 \times q_e 2) + t/q_e$, where k_2 is the pseudo-second-order rate constant of adsorption) have been used to model the kinetic adsorption. According to the correlation coefficient (R^2) in Table 1, the experimental data can be described very well by the pseudo-second-order model than by pseudo-first-order model, implying chemical adsorption as the rate-limiting step of the immobilization mechanism.

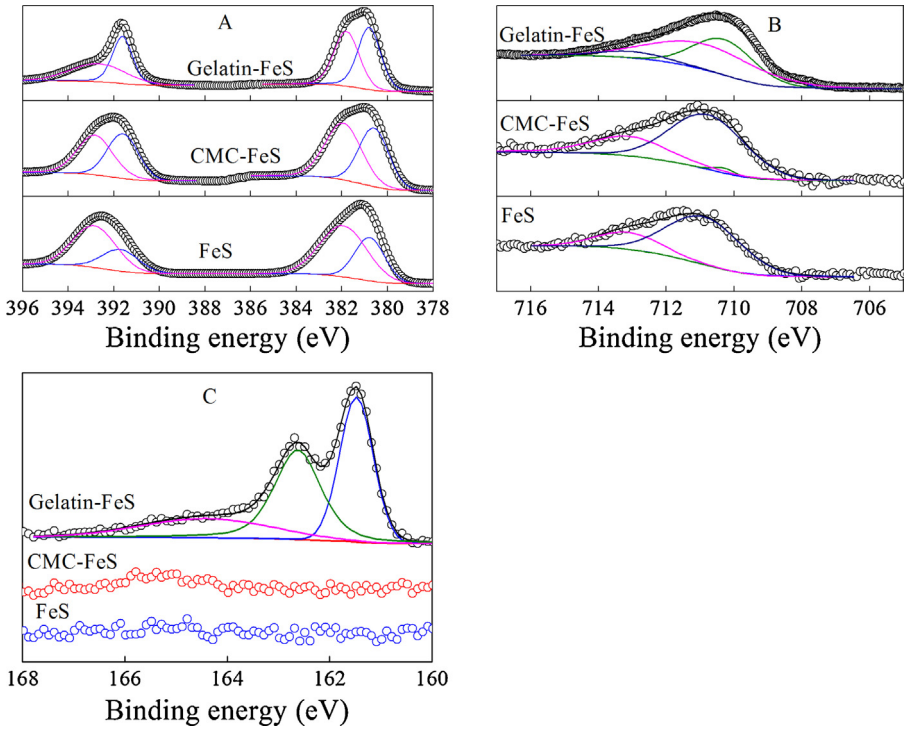

Fig. 6. XPS U 4f (A), Fe 2p (B) and S 2p (C) spectra of bare FeS, CMC–FeS and gelatin–FeS samples after U(VI) adsorption. $T = 20 \pm 1\,^{\circ}C$, contact time: 48 h, $C[U(VI)]_{(initial)} = 50.0$ mg/L, $C[FeS] = 100.0$ mg/L, pH 5.0 ± 0.1, $C[NaCl] = 0.10$ mol/L.

Table 2
Parameters of Langmuir and Freundlich models.

	Langmuir model			Freundlich model		
	q_{smax} (mg/g)	b (L/mg)	R^2	K (mg/g)	$1/n$	R^2
FeS	314.1	0.264	0.993	119.2	0.235	0.926
CMC–FeS	430.3	0.253	0.999	153.8	0.250	0.911
Gelatin–FeS	555.9	0.532	0.995	246.2	0.213	0.892

3.3.2. Adsorption isotherms

The enrichment capabilities of CMC–FeS and gelatin–FeS nanoparticles are critical for its potential application. As shown in Fig. 5B, the adsorption isotherm of U(VI) on gelatin–FeS was highest, followed by that of U(VI) on CMC–FeS nanoparticles, which was much higher than that on bare FeS. The —NH_2 and —COOH groups from gelatin can act as efficient anchor for U(VI), which may attribute to the highest adsorption capacity of gelatin–FeS for U(VI) [32]. The experimental data were fitted with the common used Langmuir model ($q_s = b \times q_{smax} \times C_e/(1 + b \times C_e)$, q_{smax} is the maximum enrichment capacity, b is Langmuir constant) and Freundlich model ($q_s = K \times {C_e}^{1/n}$, K and $1/n$ are the constants indicative of enrichment capacity and enrichment intensity), respectively. According to the correlation coefficients (R^2) in Table 2, the experimental data could be better described by the Langmuir model than by the Freundlich model. The applicability of the Langmuir model indicated that FeS, CMC–FeS and gelatin–FeS nanoparticles surfaces are uniform and homogeneous for U(VI) removal. Based on the Langmuir model, the maximum enrichment capacity (q_{smax}) of U(VI) on FeS, CMC–FeS, and gelatin–FeS at pH 5.0 were calculated to be ~314, ~430, and ~556 mg/g, respectively, which were comparable to today's nano-materials under similar experimental conditions. This observation highlighted the potential application of gelatin–FeS and CMC–FeS as adsorbents for the uptake of U(VI) from aqueous solutions in radioactive pollution cleanup.

3.3.3. Proposed mechanisms

In order to get a better understanding the effect of stabilizer on U(VI) enrichment on FeS nanoparticles, the bare FeS, CMC–FeS and gelatin–FeS samples after U(VI) adsorption were characterized by XPS technique. The XPS U 4f of U-laden FeS (Fig. 6A) was sound determined and can be quantitatively deconvoluted into U(IV) (centered at 380.7 ± 0.1 eV and 391.7 ± 0.1 eV) and U(VI) (centered at 381.9 ± 0.1 and 392.8 ± 0.1 eV) [6,9,32,33]. The ratios of U(IV):U(VI) were determined from the U 4f peaks at 380.7 ± 0.1 eV and 381.9 ± 0.1 eV (Table 3). It is noteworthy that the ratios of U(IV):U(VI) for U-laden bare FeS, CMC–FeS and gelatin–FeS samples were 0.54, 0.81 and 1.07, respectively. The results indicated that U(VI) was partly reduced to U(IV) followed the adsorption process, and the immobilized uranium on FeS nanoparticles existed as U(IV)/U(VI) mixture species. Meanwhile, the XPS Fe 2p of U-laden FeS (Fig. 6B) can be quantitatively deconvoluted into FeS (centered at 707.8 ± 0.1 eV and 710.4 ± 0.1 eV), Fe(III)-S/Fe(II)-S (centered at 710.8 ± 0.1 eV), and Fe(III)-O (centered at 713.1 ± 0.1 eV) (Table 4) [6,9]. It is noteworthy that FeS is the important species on the surface of U-laden gelatin–FeS, and is the negative species on the surfaces of U-laden bare FeS and CMC–FeS, which is further confirmed by XPS S 2p spectra. Only the XPS S 2p of U-laden gelatin–FeS (Fig. 6C) can be detected and can be deconvoluted into FeS (centered at 161.48 eV) and polysulfide (centered at 162.62 eV), and SO_4^{2-} (centered at 164.40 eV) [6,9].

The adsorption–reduction immobilization of U(VI) was reported as the major reaction mechanism for the enrichment of U(VI) by reductive materials, such as sulfate reducing biofilms [4], iron sulfide materials [9], and zero valent iron [34]. In the anoxic environment, immobilization process of U(VI) by FeS consisted of two stages: (1) adsorption of U(VI) by FeS, together with the release of Fe(II); (2) reduction of U(VI) by S^{2-} and Fe(II), forming $U_3O_8/U_4O_9/UO_2$ on FeS surfaces [6]. The abundant —NH_2 and—COOH groups in gelatin provided rich active sites not only for anchoring U(VI) and binding S^{2-} and Fe(II), which were the reductant for adsorption–reduction immobilization of U(VI), but

Table 3
Curve-fitting results of XPS U 4f spectra.

	Peak	BE[a] (eV)	FWHM[b] (eV)	Relative fraction (%)	R(U(IV)/U(VI))
FeS	U(IV)	380.78	1.54	35.2	0.54
	U(VI)	381.94	2.43	64.8	
CMC–FeS	U(IV)	380.60	1.54	44.9	0.81
	U(VI)	381.94	1.87	55.1	
Gelatin–FeS	U(IV)	380.80	1.19	51.6	1.07
	U(VI)	381.80	1.31	48.4	

[a] Binding energy.
[b] Full width at half-maximum.

Table 4
Curve-fitting results of XPS Fe 2f spectra.

	Peak	BE (eV)	FWHM (eV)	Relative fraction (%)
FeS	Fe(II)	707.70	3.86	1.41
	Fe(II)	710.50	3.22	0.00
	Fe(III)-S/Fe(II)-S	710.90	2.58	75.4
	Fe(III)-O	713.10	2.24	23.2
CMC–FeS	Fe(II)	707.82	3.60	0.00
	Fe(II)	710.30	0.74	1.75
	Fe(III)-S/Fe(II)-S	710.78	2.60	68.9
	Fe(III)-O	713.10	2.61	29.3
Gelatin–FeS	Fe(II)	707.75	0.17	0.37
	Fe(II)	710.30	2.11	40.1
	Fe(III)-S/Fe(II)-S	710.90	3.79	51.9
	Fe(III)-O	713.00	2.25	7.65

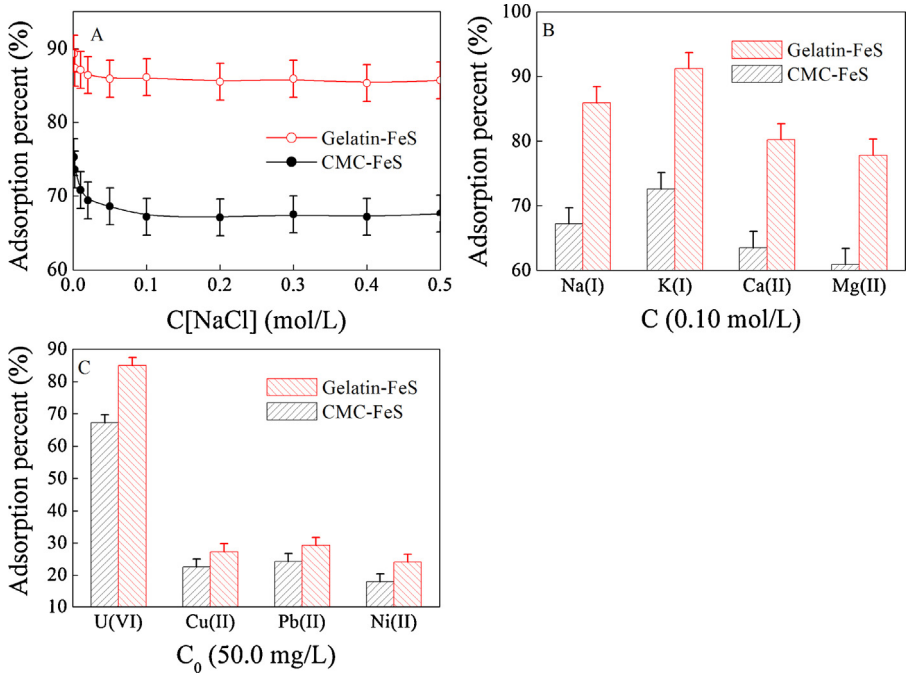

Fig. 7. Effects of salinity (A, B) on U(VI) uptake by CMC–FeS and gelatin–FeS, and the comparison of the enrichment performance of CMC–FeS and gelatin–FeS for 50.0 mg/L U(VI) and heavy metal ions (C). $T = 20 \pm 1$ °C, contact time: 48 h, C[FeS] = 100.0 mg/L, pH 5.0 ± 0.1. (A and B) $C[U(VI)]_{(initial)}$ = 50.0 mg/L. (C) C[NaCl] = 0.10 mol/L.

also for binding FeS nanoparticles, which can inhibit U(IV) reoxidation by oxygen [10]. Thereby, the ratio of U(IV):U(VI) for U-laden gelatin–FeS samples was highest.

3.4. Effect of salinity on immobilization capacity of CMC–FeS and gelatin–FeS for U(VI)

Due to the competitive effect of coexisting ions and a wide range of salinity in aqueous solutions, salinity is an important environmental factor that affects the uptake and separation of U(VI) from aqueous solution. We selected the concentration of NaCl in range of 0.001–0.5 mol/L to investigate the effect of cation concentration on U(VI), which is about 4–2380 times higher than that of U(VI) in this paper. As depicted in Fig. 7A, no notable effect of ionic strength on U(VI) uptake by CMC–FeS and gelatin–FeS was observed at the NaCl concentration of ≥0.1 mol/L, indicating that CMC–FeS and gelatin–FeS nanoparticles presented excellent tolerance to salinity. Moreover, 0.1 mol/L NaCl, KCl, $CaCl_2$, and $MgCl_2$ were also selected

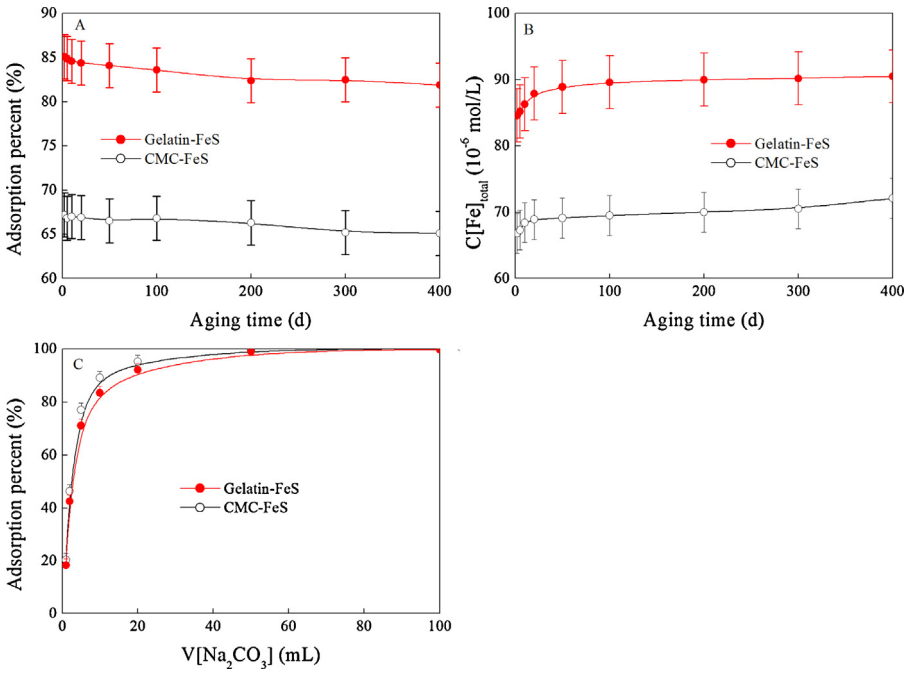

Fig. 8. Effects of aging time on U(VI) uptake by CMC–FeS and gelatin–FeS (A) and on Fe concentrations released from U-laden gelatin–FeS and CMC–FeS (B), and the kinetic desorption of U(VI) by eluting 10 mg U-laden gelatin–FeS and CMC–FeS with 0.1 mol/L Na_2CO_3 (C). (A, B) $T = 20 \pm 1$ °C, $C[U(VI)]_{(initial)} = 50.0$ mg/L, $C[FeS] = 100.0$ mg/L, pH 5.0 ± 0.1, $C[NaCl] = 0.10$ mol/L.

to study the effect of different cations on U(VI) adsorption because Na(I), K(I), Ca(II) and Mg(II) are widely exist in aqueous solutions [35,36]. As can be seen from Fig. 7B, ~61% and ~78% of U(VI) was extracted by CMC–FeS and gelatin–FeS in the presence of 0.1 mol/L Mg(II), respectively. The reduced adsorption efficiency Ca(II) and Mg(II) can be due to the ternary complexes formed by U(VI), CO_3^{2-}, and Ca(II)/Mg(II) [35,36]. Furthermore, CMC–FeS and gelatin–FeS also present excellent selectivity for U(VI) against other coexisting heavy metal ions (such as Pb(II), Cu(II), and Ni(II)) from aqueous solutions under the experimental conditions (Fig. 7C). Thereby, CMC–FeS and gelatin–FeS nanoparticles can be used as promising materials to uptake trace U(VI) from large volume of real aqueous solutions.

3.5. Long-term stability of U(VI) immobilized by CMC–FeS and gelatin–FeS

For engineered remediation applications, the long term stability of immobilized U(VI) is critical for the real application of CMC–FeS and gelatin–FeS as candidate materials for the uptake of U(IV) from aqueous solutions. It is widely believed that besides surface adsorption, partial reduction of U(VI)–U(IV) and/or the precipitation of U(IV)/U(VI) are important mechanisms of U(VI) immobilization on FeS surface [7,9]. The long-term effective immobilization of U(VI) is fairly depends on the stability of U(IV)/U(VI) materials [1]. However, partial reoxidation of U(IV) can be occurred even under sustained reducing conditions [37]. Fig. 8A depicts the effects of aging time on U(VI) adsorption. After 400 d of aging at room temperature, U(VI) adsorption percent was slightly decreased by ~2–3%, e.g. from ~67% to ~65% and from ~85% to ~82% on the surface of CMC–FeS and gelatin–FeS, respectively. The slightly decreased U(VI) adsorption can be due to the reoxidation of U(IV) by oxidants such as dissolved oxygen even under sustained reducing conditions [1,10,37,38]. The enrichment of U(VI) by FeS nanoparticles was accompanied by the release of ferric ions into aqueous solutions [6]. Our observation (Fig. 8B) supports this. As shown in Fig. 8B, the total Fe concentrations were sound increased by $\sim 5 \times 10^{-6}$ mol/L after aging for 400 days.

3.6. Desorption and recovery of uranium ions

The kinetic desorption and recovery of U(VI) was also measured by eluting 10 mg U-laden gelatin–FeS and CMC–FeS with 0.1 mol/L Na_2CO_3, which can form complexes with U(VI). The desorption efficiency vs the volume of Na_2CO_3 is shown in Fig. 8C, which clearly illustrates that 0.1 mol/L Na_2CO_3 was enough for the quantitative desorption of uranium ions from the surfaces of gelatin–FeS and CMC–FeS in for potential applications.

4. Conclusions

In summary, gelatin not only can effectively prevent agglomeration of FeS nanoparticles, but also can provide abundant functional groups, and thereby facilitate preparation of highly stable and soil deliverable FeS nanoparticles with highest immobilization capacity for U(VI). This paper highlighted the applicability of gelatin–FeS in aqueous solutions in radioactive uranium contaminant cleanup.

Acknowledgments

The financial support from the National Natural Science Foundation of China (21307135, 91326110, 21225730, 91326202), NSAF (1U1530131), Anhui Provincial Natural Science Foundation (1508085MB29), the Science Foundation of Institute of Plasma Physics, Chinese Academy of Sciences (DSJJ-13-YY01), the Radiochemistry 909 Project in the China Academy of Engineering Physics, the Science and Technology Development Foundation of China Academy of Engineering Physics (2014B0301034) are acknowledged.

References

[1] Y. Bi, S.P. Hyun, R.K. Kukkadapu, K.F. Hayes, Oxidative dissolution of UO_2 in a simulated groundwater containing synthetic nanocrystalline mackinawite, Geochim. Cosmochim. Acta 102 (2013) 175–190.
[2] F. Dullies, W. Lutze, W. Gong, H.E. Nuttall, Biological reduction of uranium—from the laboratory to the field, Sci. Total Environ. 408 (2010) 6260–6271.

[3] X. Tan, X. Ren, C. Chen, X. Wang, Analytical approaches to the speciation of lanthanides at solid–water interfaces, TrAC-Trend Anal. Chem. 61 (2014) 107–132.
[4] H. Beyenal, R.K. Sani, B.M. Peyton, A.C. Dohnalkova, J.E. Amonette, Z. Lewandowski, Uranium immobilization by sulfate-reducing biofilms, Environ. Sci. Technol. 38 (2004) 2067–2074.
[5] J.R. Bargar, K.H. Williams, K.M. Campbell, P.E. Long, J.E. Stubbs, E.I. Suvorova, J.S. Lezama-Pacheco, D.S. Alessi, M. Stylo, S.M. Webb, J.A. Davis, D.E. Giammar, L.Y. Blue, R. Bernier-Latmani, Uranium redox transition pathways in acetate-amended sediments, PNAS 110 (2013) 4506–4511.
[6] B. Hua, B. Deng, Reductive immobilization of uranium(VI) by amorphous iron sulfide, Environ. Sci. Technol. 42 (2008) 8703–8708.
[7] C. Bruggeman, N. Maes, Uptake of uranium(VI) by pyrite under boom clay conditions: influence of dissolved organic carbon, Environ. Sci. Technol. 44 (2010) 4210–4216.
[8] J.L. Druhan, M.E. Conrad, K.H. Williams, L. N'Guessan, P.E. Long, S.S. Hubbard, Sulfur isotopes as indicators of amended bacterial sulfate reduction processes influencing field scale uranium bioremediation, Environ. Sci. Technol. 42 (2008) 7842–7849.
[9] T.B. Scott, O.R. Tort, G.C. Allen, Aqueous uptake of uranium onto pyrite surfaces: reactivity of fresh versus weathered material, Geochim. Cosmochim. Acta 71 (2007) 5044–5053.
[10] Y. Bi, K.F. Hayes, Nano-FeS inhibits UO_2 reoxidation under varied oxic conditions, Environ. Sci. Technol. 48 (2014) 632–640.
[11] T.J. Gallegos, C.C. Fuller, S.M. Webb, W. Betterton, Uranium(VI) interactions with mackinawite in the presence and absence of bicarbonate and oxygen, Environ. Sci. Technol. 47 (2013) 7357–7364.
[12] Z. Xiong, F. He, D. Zhao, M.O. Barnett, Immobilization of mercury in sediment using stabilized iron sulfide nanoparticles, Water Res. 43 (2009) 5171–5179.
[13] C. Wittekindt, D. Marx, Water confined between sheets of mackinawite FeS minerals, J. Chem. Phys. 137 (2012) 054710.
[14] C. Xu, Y. Zeng, X. Rui, N. Xiao, J. Zhu, W. Zhang, J. Chen, W. Liu, H. Tan, H.H. Hng, Q. Yan, Controlled soft-template synthesis of ultrathin C@FeS nanosheets with high-Li-storage performance, ACS Nano 6 (2012) 4713–4721.
[15] Y. Gong, Y. Liu, Z. Xiong, D. Zhao, Immobilization of mercury by carboxymethyl cellulose stabilized iron sulfide nanoparticles: reaction mechanisms and effects of stabilizer and water chemistry, Environ. Sci. Technol. 48 (2014) 3986–3994.
[16] N. Sakulchaicharoen, D.M. O'Carroll, J.E. Herrera, Enhanced stability and dechlorination activity of pre-synthesis stabilized nanoscale FePd particles, J. Contam. Hydrol. 118 (2010) 117–127.
[17] F. He, D. Zhao, Manipulating the size and dispersibility of zerovalent iron nanoparticles by use of carboxymethyl cellulose stabilizers, Environ. Sci. Technol. 41 (2007) 6216–6221.
[18] F. He, D. Zhao, J. Liu, C.B. Roberts, Stabilization of Fe–Pd nanoparticles with sodium carboxymethyl cellulose for enhanced transport and dechlorination of trichloroethylene in soil and groundwater, Ind. Eng. Chem. Res. 46 (2007) 29–34.
[19] M. Zhang, Y. Wang, D. Zhao, G. Pan, Immobilization of arsenic in soils by stabilized nanoscale zero-valent iron iron sulfide (FeS), and magnetite (Fe_3O_4) particles, Chin. Sci. Bull. 55 (2010) 365–372.
[20] F. He, D. Zhao, Preparation and characterization of a new class of starch-stabilized bimetallic nanoparticles for degradation of chlorinated hydrocarbons in water, Environ. Sci. Technol. 39 (2005) 3314–3320.
[21] X. Ma, F. Xu, X. Wang, Y. Du, L. Chen, Z. Zhang, The U-shaped $Fe_{(1-x)}S$ micro-slots: growth, characterization, and magnetic property, J. Cryst. Growth 277 (2005) 314–320.
[22] K. Larson-Smith, D.C. Pozzo, Pickering emulsions stabilized by nanoparticle surfactants, Langmuir 28 (2012) 11734–11741.
[23] Y. Gong, Y. Liu, Z. Xiong, D. Kaback, D. Zhao, Immobilization of mercury in field soil and sediment using carboxymethyl cellulose stabilized iron sulfide nanoparticles, Nanotechnology 23 (2012) 294007.
[24] B. Gaihre, M.S. Khil, H.K. Kang, H.Y. Kim, Bioactivity of gelatin coated magnetic iron oxide nanoparticles: in vitro evaluation, J. Mater. Sci. Mater. Med. 20 (2009) 573–581.
[25] J.M.A. Almeida, C.T. Meneses, A.S. Menezes, R.F. Jardim, J.M. Sasaki, Synthesis and characterization of $NiMn_2O_4$ nanoparticles using gelatin as organic precursor, J. Magn. Magn. Mater. 320 (2008) e304–e307.
[26] B. Gaihre, S. Aryal, N.A.M. Barakat, H.Y. Kim, Gelatin stabilized iron oxide nanoparticles as a three dimensional template for the hydroxyapatite crystal nucleation and growth, Mater. Sci. Eng. C 28 (2008) 1297–1303.
[27] M.R. Hansen, A. Blennow, I. Farhat, L. Norgaard, S. Pedersen, S.B. Engelsen, Comparative NMR relaxometry of gels of amylomaltase-modified starch and gelatin, Food Hydrocolloids 23 (2009) 2038–2048.
[28] S.S. Thakur, G.S. Chauhan, Gelatin–silica-based hybrid materials as efficient candidates for removal of chromium(VI) from aqueous solutions, Ind. Eng. Chem. Res. 53 (2014) 4838–4849.
[29] B. Gaihre, M.S. Khil, D.R. Lee, H.Y. Kim, Gelatin-coated magnetic iron oxide nanoparticles as carrier system: drug loading and in vitro drug release study, Int. J. Pharm. 365 (2009) 180–189.
[30] W. Wei, R. Sun, Z. Jin, J. Cui, Z. Wei, Hydroxyapatite–gelatin nanocomposite as a novel adsorbent for nitrobenzene removal from aqueous solution, Appl. Surf. Sci. 292 (2014) 1020–1029.
[31] S. Zhang, H. Niu, Y. Cai, X. Zhao, Y. Shi, Arsenite and arsenate adsorption on coprecipitated bimetal oxide magnetic nanomaterials: $MnFe_2O_4$ and $CoFe_2O_4$, Chem. Eng. J. 158 (2010) 599–607.
[32] D. Shao, X. Wang, J. Li, Y. Huang, X. Ren, G. Hou, X. Wang, Reductive immobilization of uranium by PAAM-FeS/Fe_3O_4 magnetic composites, Environ. Sci. Water Res. Technol. 1 (2015) 169–176.
[33] Q. Wu, B.V. Yakshinskiy, T. Gouder, T.E. Madey, H_2S adsorption on polycrystalline UO_2, Catal. Today 85 (2003) 291–301.
[34] R.A. Crane, M. Dickinson, I.C. Popescu, T.B. Scott, Magnetite and zero-valent iron nanoparticles for the remediation of uranium contaminated environmental water, Water Res. 45 (2011) 2931–2942.
[35] D. Shao, G. Hou, J. Li, T. Wen, X. Ren, X. Wang, PANI/GO as a super adsorbent for the selective adsorption of uranium(VI), Chem. Eng. J. 255 (2014) 604–612.
[36] D. Shao, J. Li, X. Wang, Poly(amidoxime)-reduced graphene oxide composites as adsorbents for the enrichment of uranium from seawater, Sci. China B 57 (2014) 1449–1458.
[37] J.M. Wan, T.K. Tokunaga, E. Brodie, Z.M. Wang, Z.P. Zheng, D. Herman, T.C. Hazen, M.K. Firestone, S.R. Sutton, Reoxidation of bioreduced uranium under reducing conditions, Environ. Sci. Technol. 39 (2005) 6162–6169.
[38] Y. Bi, K.F. Hayes, Surface passivation limited UO_2 oxidative dissolution in the presence of FeS, Environ. Sci. Technol. 18 (2014) 13402–13411.